Supplementary information for

Enhancing hydrogen production of microalgae by redirecting electrons from photosystem I to hydrogenase

Sigrun Rumpel, Judith F. Siebel, Christophe Farès, Jifu Duan, Edward Reijerse, Thomas Happe, Wolfgang Lubitz and Martin Winkler

Abbreviations

$PETF^{ox}$: oxidized PETF

$PETF^{red}$: reduced PETF

Identification of PETF-residues involved in complex formation with HYDA1

Titration experiments were performed with both $PETF^{ox}$ and $PETF^{red}$ as well as fully active HYDA1 and apo-HYDA1 containing only the [4Fe-4S]-part of the H-cluster[1, 2] (Fig. 1 in the main text and Figs. S1-S3). Since, not unexpectedly, the titration of $PETF^{red}$ with active HYDA1 was virtually identical to that of apo-HYDA1 (Fig. S1), only the apo-HYDA1 results are discussed in the main text. Both $PETF^{red}$ and $PETF^{ox}$ titrations with HYDA1 and FNR confirmed the previously identified binding surfaces (Table S1). Interestingly, $\Delta\delta_{HN}$ for $PETF^{red}$ were increased about 4-fold compared to $PETF^{ox}$ and almost unchanged at a 3-times lower excess of HYDA1 (Fig. 1 in the main text and Fig. S2b) indicating a higher affinity of $PETF^{red}$ than $PETF^{ox}$ for HYDA1. For $PETF^{red}$, the additionally significant $\Delta\delta_{HN}$ for residues G47-V49, F71 and Y78 are probably secondary effects due to a conformational change in the neighboring regions (Y35-C45 and L73-V76) that coordinate the [2Fe-2S]-cluster. This conformational change is most likely related to electron transfer from $PETF^{red}$ to HYDA1. Surprisingly, the larger difference in the observed $\Delta\delta_{HN}$ for D19 and D58 is more pronounced for $PETF^{ox}$ than for $PETF^{red}$ although $PETF^{red}$ forms the reactive electron transfer complex (Fig. S3).

Table S1 | Summary of the largest chemical shift perturbations of PETF upon FNR and HYDA1 addition and shortest intermolecular distance for the PETF/FNR complex structure 1GAQ. PETF residues identified as important for protein binding are labelled by grey background.

PETF			PETF/FNR complex[a]	
$\Delta\delta_{HN}$ (ppm) upon HYDA1-binding	**residue**	$\Delta\delta_{HN}$ (ppm) upon FNR-binding	residue(s) closest to the PETF residue	minimum distance (Å)
0.003	**D19**	0.055	E19[c]	11.9
0.004	**Y21**	0.025	K153	5.4
0.007	**L23**[3]	0.016	E154	6.1
0.014	**D24**[2]	0.014	E154	6.5
0.009	**A25**[10]	0.019	K301	6.9
0.013	**E27**[2]	0.01	K301, K304	3.4, 3.1
0.009	**E28**[2]	0.013	K301, R305	1.7, 3.8
0.005	**A29**[10]	0.008	K301	3.8
0.001	**G30**[10, 11]	0.014	K301, F297	4.2, 5
0.007	**L31**	0.01	K301	6.3
0.005	**D32**	0.011	F297	3.8
0.006	**V54**	0.014	K35	13.8
0.005	**D55**	0.019	K33	10.4
0.002	**Q56**	0.025	K33	7.2
0.003	**S57**[10]	0.007	K33	4.5
0.006	**D58**[2, 10]	0.042	N30, K33, K153	3.1, 3.4, 4.9
0.012	**Q59**[10]	0.015	K35, K33	2.8, 3.8
disappeared	**S60**[2]	disappeared	N30, K33, P34	2.5, 3.2, 2.3
disappeared	**F61**[2]	disappeared	V92	2.2
0.034	**L62**[10, 11]	0.034	K91, K35	4.3, 4.9
0.013	**D63**[2, 10]	0.02	K91	2
0.02	**D64**[10]	0.017	K88	2.6
0.021	**A65**[10]	0.017	K88	5.1
0.03	**Q66**	0.018	K91	2.9
0.006	**Y78**	0.015	K153	8.3
0.006	**H88**[3]	0.011	K275	7.8
0.01	**Q89**[3]	0.01	K275	10.2
0.02	**E90**[2]	0.011	K88, K91	7.2, 7.2
0.004	**E91**[2]	0.007	K88	7.2
0.005	**A92**	0.027	R93, Y120	7.6, 7.2
0.062	**L93**	0.046	K85	4.9
0.04	**Y94**[10, 11]	0.041	N86	5.8

[a]based on the X-ray structure for the PETF/FNR complex from *maize leaf* (1GAQ).

[b]E19 is the N-terminal residue of FNR in 1GAQ. 18 N-terminal residues are missing in the X-ray structure.

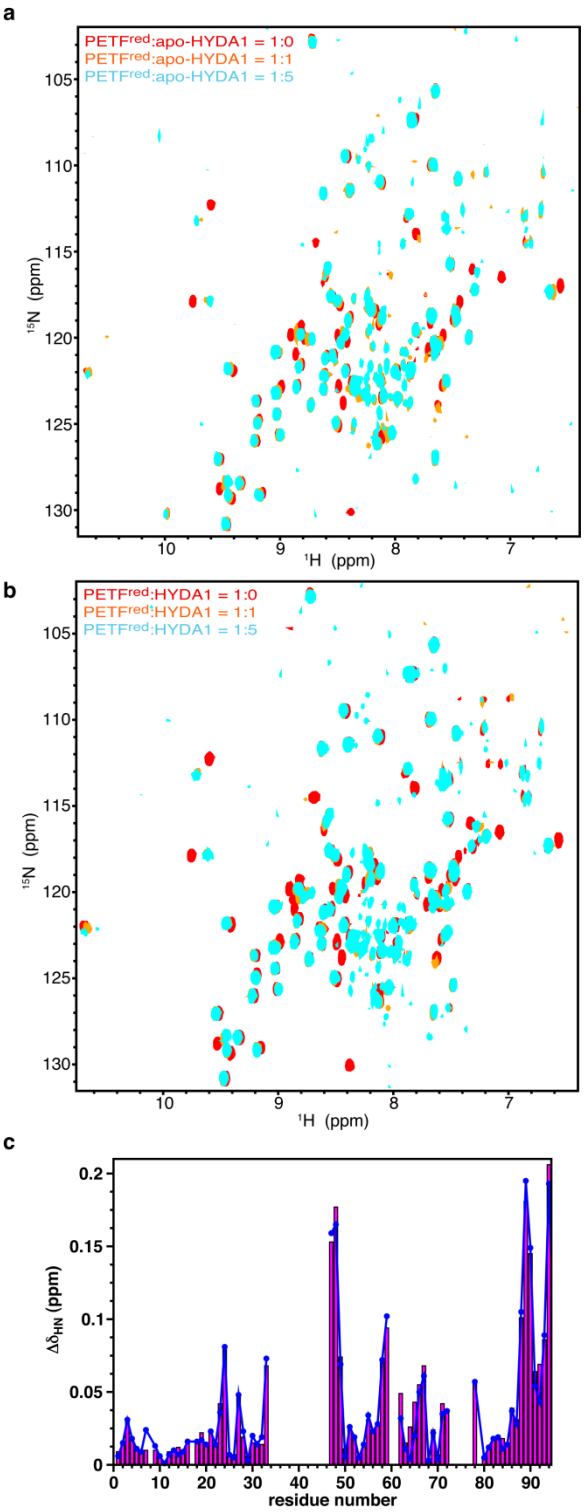

Fig. S1 | (a,b) Overlay of ^{1}H-^{15}N TROSY-HSQC spectra of PETF^{red} with binding partner at ratios of 1:0 (red), 1:1 (orange) and 1:5 (cyan) shown for PETF^{red}:apo-HYDA1 (**a**) and PETF^{red}: active HYDA1 (**b**). (**c**) Weighted averages of the ^{1}H and ^{15}N backbone chemical shift changes plotted versus the residue number at a 5-fold excess of apo-HYDA1 (blue line) and active HYDA1 (magenta bars) upon binding to PETF^{red}.

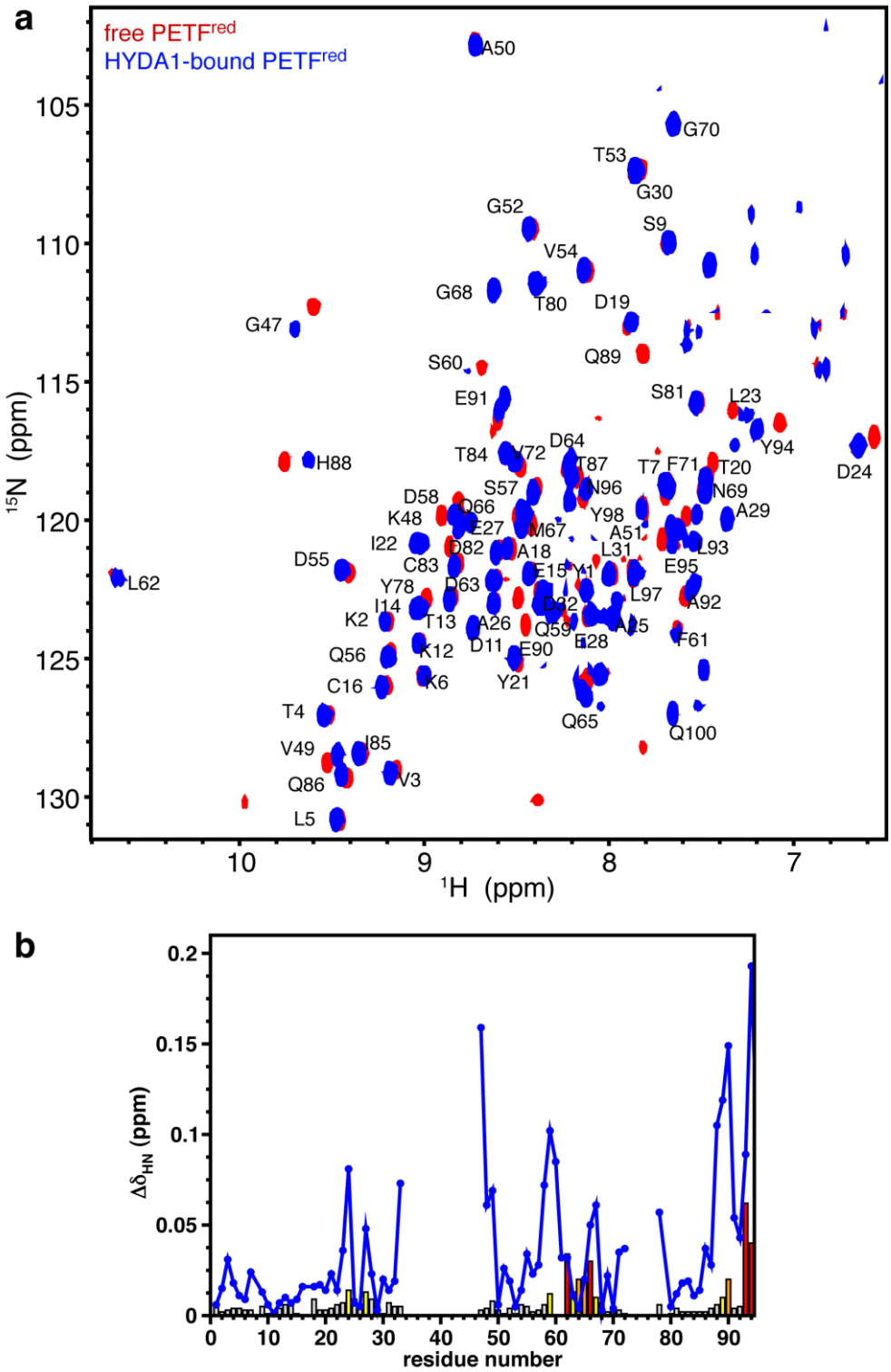

Fig. S2 | (**a**) Overlay of ^{1}H-^{15}N TROSY-HSQC spectra of ^{15}N-labelled PETF^{red} in the absence (red) and presence (blue) of HYDA1 at a 1:1 molar ratio. (**b**) Amide backbone chemical shift changes of PETF^{ox} and PETF^{red} upon HYDA1-binding. Weighted averages of the ^{1}H and ^{15}N backbone chemical shift changes plotted versus the residue number at a 15-fold excess of HYDA1 for PETF^{ox} (bars) and a 5-fold excess of HYDA1 for PETF^{red} (blue line). The coloured bars correspond to **Fig. 3**.

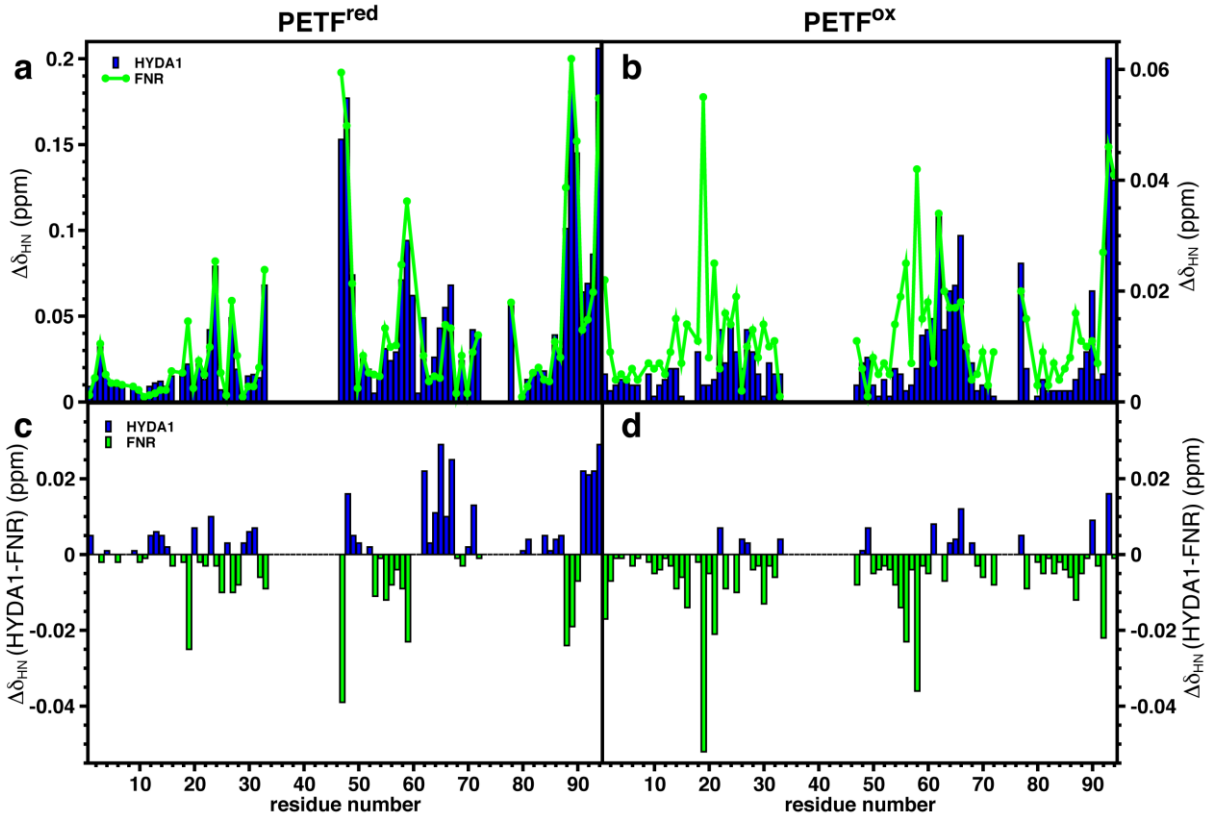

Fig. S3 | Differences between HYDA1- and FNR-binding to PETF^{red} and PETF^{ox}. Weighted averages of the amide backbone ^{1}H and ^{15}N chemical shift changes ($\Delta\delta_{HN}$) upon protein binding are plotted versus the residue number for PETF^{red} (**a**,**c**) and for PETF^{ox} (**b,d**). (**a,b**) Chemical shift changes between free and bound PETF are calculated for a 5- and 15-fold excess of binding partner, respectively. Bars indicating the results for HYDA1 are colored blue and green lines indicate results obtained with FNR. (**c**,**d**) Differences of the average chemical shift changes for FNR- and HYDA1-binding were determined as $\Delta\delta_{HN}$(HYDA1)-$\Delta\delta_{HN}$(FNR) and residues with larger chemical shift changes for HYDA1 are shown as blue bars and as green bars for FNR.

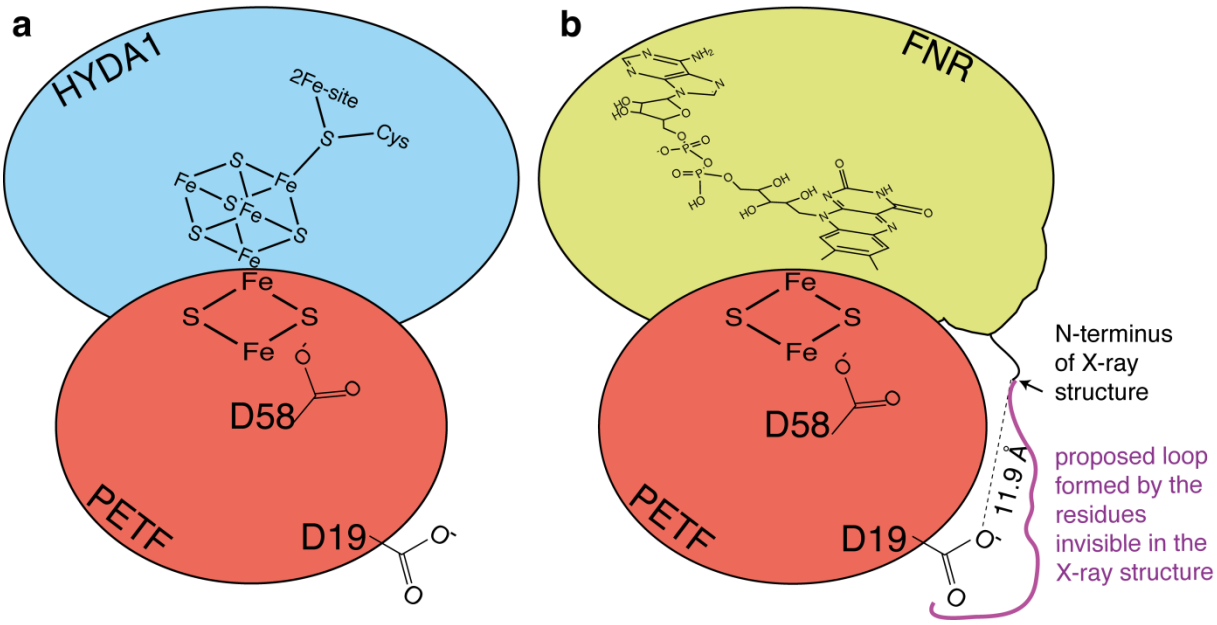

Fig. S4 | Schematic representation of the PETF/HYDA1 (a) and the PETF/FNR complex (b).

```
                          D19                                   D58
PETFCr  YKVTL--KTPSGDKTIECPADTYILDAAEEAGLDLPYSCRAGACSSCAGKVAAGTVDQSDQSFLDDAQMGNGFVLTCVAYPTSDCTIQTHQEEALY-
FDX Vc  YKVTF--KTPSGDKVVEVADDVYLLDAAEEAGMDLPYSCRAGACSSCAGKIVSGTVDQSDQSFLDDKQMEAGFVLTCVAYATSDLVILTNQEEGLY-
FDX Cf  YKVTL--KTPSGEETIECPEDTYILDAAEEAGLDLPYSCRAGACSSCAGKVESGEVDQSDQSFLDDAQMGKGFVLTCVAYPTSDVTILTHQEAALY-
FDX Ds  YMVTL--KTPSGEQKVEVSPDSYILDAAEEAGVDLPYSCRAGSCSSCAGKVESGTVDQSDQSFLDDDQMDSGFVLTCVAYATSDCTIVTHQEENLY-
FDX At  YKVKFI--TPEGEQEVECEEDVYVLDAAEEAGLDLPYSCRAGSCSSCAGKVVSGSIDQSDQSFLDDEQMSEGYVLTCVAYPTSDVVIETHKEEAIM-
FDX Zm  YNVKLI--TPEGEVELQVPDDVYILDQAEEDGIDLPYSCRAGSCSSCAGKVVSGSVDQSDQSYLDDGQIADGWVLTCHAYPTSDVVIETHKEEELTGA
FDX Ps  YKVKLV--TPDGTQEFECPSDVYILDHAEEVGIDLPYSCRAGSCSSCAGKVVGGEVDQSDGSFLDDEQIEAGFVLTCVAYPTSDVVIETHKEEDLTA-
FDX S   YTVKLI--TPDGESSIECSDDTYILDAAEEAGLDLPYSCRAGACSTCAGKITAGSVDQSDQSFLDDDQIEAGYVLTCVAYPTSDCTIETHKEEDLY-
FDX N   FKVTLINEAEGTKHEIEVPDDEYILDAAEEQGYDLPFSCRAGACSTCAGKLVSGTVDQSDQSFLDDDQIEAGYVLTCVAYPTSDVVIQTHKEEDLY-
FDX Te  YKVTLV-RPDGSETTIDVPEDEYILDVAEEQGLDLPFSCRAGACSTCAGKLLEGEVDQSDQSFLDDDQIEKGFVLTCVAYPRSDCKILTNQEEELY--
```

Fig. S5 | Sequence alignment of different plant-type ferredoxins. PETF sequences of different photosynthetic organisms are compared comprising representative species from algae, higher plants and cyanobacteria. N-terminal sequence parts have been trimmed in reference to the sequence homology to mature PETF*Cr* excluding the chloroplast transit peptide. Positions D19 and D58 of PETF*Cr* which promote selective recognition of FNR are indicated by a magenta background colour. A yellow background marks cysteine residues that participate in the ligation of the [2Fe-2S]-cluster. Other parts with strict sequence conservancy are indicated by a grey background colour. PETF*Cr*: ferredoxin I of *C. reinhardtii* (protein ID: XP_001692808), FDX *Vc*: ferredoxin I of *Volvox carteri f. nagariensis* (protein ID: XP_002958725), FDX *Cf*: Ferredoxin of *Chlorella fusca* (protein ID: P56408), FDX *Ds*: ferredoxin I of *Dunaliella salina* (protein ID: P00239), FDX *At*: ferredoxin I of *Arabidopsis thaliana* (protein ID: NP_172565), FDX *Zm*: ferredoxin 1 of *Zea mays* (protein ID: NP_001105345), FDX *Ps*: ferredoxin I of *Pisum sativum* (protein ID: P09911), FDX *S*: ferredoxin I of *Synecocystis* sp. PCC 6803 (protein ID: NP_442127), FDX *N*: ferredoxin I of *Nostoc* sp. PCC 7120 (protein ID: NP_488188), FDX *Te* : ferredoxin I of *Thermosynechococcus elongatus* BP-1 (protein ID: NP_681799).

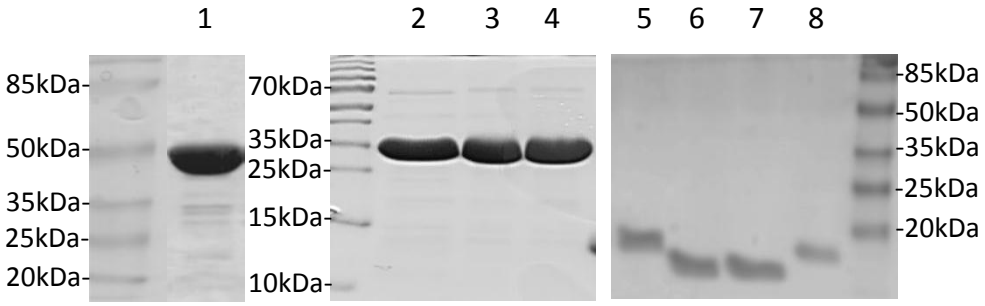

Fig. S6 | Analysis of purified proteins by SDS–PAGE visualized by Coomassie staining. 1: 30 µg HYDA1; 2: 25 µg wt-FNR; 3: 25 µg FNR-K83L; 4: 25 µg FNR-K89L; 5: 7 µg wt-PETF; 6: 7 µg PETF-D58A; 7: 7 µg PETF-D19A/D58A; 8: 5 µg PETF-D19A.

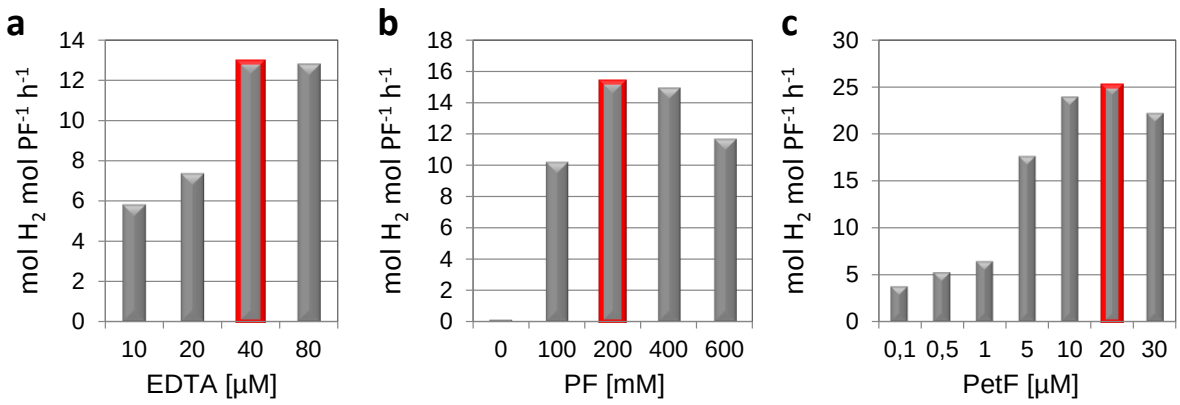

Fig. S7 | Adjustment of compound concentrations of the proflavine dependent *in vitro* assay for light-driven H_2 production. Test series with increasing concentrations of EDTA, PF and PETF were screened for the highest yield of photoproduced H_2. The indicated concentrations (red framed bars) were chosen as standard system parameters for all PF-dependent measurements.

References

1. D. W. Mulder, E. S. Boyd, R. Sarma, R. K. Lange, J. A. Endrizzi, J. B. Broderick and J. W. Peters, *Nature*, 2010, **465**, 248-251.
2. J. Esselborn, C. Lambertz, A. Adamska-Venkatesh, T. Simmons, G. Berggren, J. Noth, J. Siebel, A. Hemschemeier, V. Artero, E. Reijerse, M. Fontecave, W. Lubitz and T. Happe, *Nat. Chem. Biol.*, 2013, **9**, 607-609.
3. M. Winkler, S. Kuhlgert, M. Hippler and T. Happe, *J. Biol. Chem.*, 2009, **284**, 36620-36627.
4. P. N. Palma, B. Lagoutte, L. Krippahl, J. J. G. Moura and F. Guerlesquin, *FEBS Lett.*, 2005, **579**, 4585-4590.
5. G. Kurisu, M. Kusunoki, E. Katoh, T. Yamazaki, K. Teshima, Y. Onda, Y. Kimata-Ariga and T. Hase, *Nat. Struct. Biol.*, 2001, **8**, 117-121.
6. K. Sybirna, P. Ezanno, C. Baffert, C. Léger and H. Bottin, *Int. J. Hydrogen Energy*, 2013, **38**, 2998-3002.